https://doi.org/10.5194/cp-2023-42
Preprint. Discussion started: 3 July 2023

Climate of the Past
Discussions

Late Pleistocene glacial terminations accelerated by proglacial lakes

Meike D. W. Scherrenberg[1], Constantijn J. Berends[1], Roderik S.W. van de Wal[1,2]

[1]Institute for Marine and Atmospheric research Utrecht, Utrecht University, 3584 CC Utrecht, the Netherlands
[2]Faculty of Geosciences, Department of Physical Geography, Utrecht University, Utrecht, the Netherlands

Correspondence to: M.D.W. Scherrenberg (M.D.W.Scherrenberg@uu.nl)

Abstract. During the glacial cycles of the past 800 thousand years, Eurasia and North America were periodically covered by large ice sheets. While the Late Pleistocene glacial cycles typically lasted 80 – 120 thousand years, the termination phases only took 10 thousand years to complete. During these glacial terminations, the North American and Eurasian ice sheets retreated which created large proglacial lakes in front of the ice sheet margin. Proglacial lakes accelerate the deglaciation as they can facilitate ice shelves in the southern margins of the North American and the Eurasian ice sheets. Ice shelves are characterized by basal melting, low surface elevations and negligible friction at the base. Here we quantify the effect of proglacial lakes, and the combined effect with glacial isostatic adjustment (GIA) on Late Pleistocene glacial terminations.

We find that proglacial lakes accelerate the deglaciation of the ice sheets mainly because of the absence of basal friction underneath ice shelves. If the friction underneath grounded ice is applied to floating ice, we find that full deglaciation is postponed by a few millennia, the Barents-Kara Sea region does not fully deglaciate, and there are no extensive ice shelves. Additionally, the large uncertainty in melt rates underneath lacustrine ice shelves translates to an uncertainty in the timing of the termination of only a few centuries at most.

Proglacial lakes are created by the depression in the landscape that linger after the ice sheet has retreated. The depth, size and timing of proglacial lakes depend on the bedrock rebound. We find that if the bedrock rebounds within a few centuries, instead of a few millennia, the mass loss rate of the ice sheet is substantially reduced. This is because fast bedrock rebound prevents the formation of extensive proglacial lakes. Additionally, a decrease in thickness is partly compensated by the faster bedrock rebound, resulting in a higher surface elevation with lower temperatures and higher surface mass balance delaying deglaciation. We find that a very long bedrock relaxation time does not affect terminations substantially, but will lead to a later inception of the next glacial period. This is because initial inception regions, such as North-Western Canada, remain below sea level throughout the preceding interglacial period.

1 Introduction

From paleoglaciology we can learn which processes are important for the melt of ice sheets, which can improve our understanding of the response of the Antarctic and Greenland ice sheets under future warming. During the Late Pleistocene (~800 – 10 thousand years (kyr) ago), the North American and Eurasian continents were recurrently covered by large ice sheets (Batchelor et al., 2019). While a single glacial cycle took on average 80 – 120 kyr, their decay phases only took 10 kyr. The

https://doi.org/10.5194/cp-2023-42
Preprint. Discussion started: 3 July 2023

climate underwent global-scale changes during these glacial terminations and sea levels increased by up to 130 meters (Lambeck et al., 2014; Simms et al., 2019) mostly due to mass loss of the ice sheets. As a consequence, the planetary albedo decreased due to the smaller extent of snow, sea ice and ice sheets (Clark and Tarasov, 2014). Large volumes of carbon stored in the deep ocean were released (e.g, Denton et al., 2010; Menviel, 2019; Hasenfratz et al., 2019; Sigman et al., 2021) which contributed to an increase in CO_2 concentrations by 80 – 100 parts per million (Bereiter et al., 2015). These processes and changes in insolation, which are an important pacer for glacial cycles (Milankovitch, 1941), caused global temperatures to increase by roughly 4 – 5 °C (Annan et al., 2022). While each of these processes enhanced the mass loss of the ice sheets, these glaciated regions also act as a positive and negative feedback in the deglaciation. It has for instance been suggested that the Late Pleistocene deglaciation phases only take place if the ice sheets are large enough (e.g., Abe-Ouchi et al.,2013; Berends et al., 2021; Parrenin and Paillard, 2003).

There are various ways ice sheets have a significant impact on the climate and vice versa. Regions with ice and snow have a high albedo, which increases the amount of solar irradiance that is reflected and decreases global and local temperatures. There exists an ice albedo-feedback, where albedo decrease due to the retreat of the ice sheets amplifies temperature increase and ablation. Additionally, the elevation of an ice sheet influences the surface mass balance; a surface mass balance height feedback. A decrease in surface elevation increases temperatures which enhances ablation and causes a further decrease in ice thickness. Ice sheet mass balance also depends on the amount of accumulation. The amount of precipitation may decline with elevation as decreasing temperatures lower the vapour pressure and therefore limit the available moisture content. Orographic forcing of precipitation can result in windward and leeward effects, depending on both ice-sheet geometry and prevailing winds. The ice-sheet topography can also influence large-scale atmospheric circulation (Löfverström et al., 2016), influencing both temperature and accumulation patterns (Pausata et al., 2011; Ullman et al., 2014) on a global scale.

Besides changes in the forcing, dynamical processes in the ice sheet can also influence the mass loss rates. Marine ice sheets where the grounding line rests on a retrograde slope may exhibit an instability, where a small perturbation can cause a self-sustained advance or retreat (Weertman, 1974; Schoof, 2012). This process is referred to as marine ice sheet instability (MISI) and it is thought to be especially important for the West-Antarctic ice sheet (Pattyn, 2018), which has substantial parts of its grounding line resting on retrograde slopes. In the past decade, many improvements have been made in capturing MISI in ice-sheet models (e.g, Pattyn et al., 2012, 2013; Schoof, 2007; Schoof, 2012; Sun et al., 2020). The North American and Eurasian ice sheets had large terrestrial margins. Yet, during glacial terminations these ice sheets may have undergone the lacustrine equivalent of MISI, called proglacial lake ice sheet instability (PLISI; Quiquet et al., 2021; Hinck et al., 2022). Proglacial lakes are created by the combination of glacial isostatic adjustment (GIA; Peltier, 1974) and runoff. The large mass of the ice sheet prompts bedrock deformation which creates a depression in the landscape. As the ice sheet starts to retreat, the rebound lags behind in time, creating an ice-free depression in front of the ice margin. This depression can fill up with melt water, creating a proglacial lake. Evidence for the existence of large proglacial lakes during the last deglaciation has been found in North America (Lake Agassiz; Upham, 1880; Lepper et al., 2013) and Eurasia (Baltic ice lake; Patton et al., 2017).

https://doi.org/10.5194/cp-2023-42
Preprint. Discussion started: 3 July 2023

Climate of the Past Discussions

Recently, Hinck et al. (2022) and Quiquet et al. (2021) have used an ice sheet model to study the deglaciation of North America using PLISI. They showed that proglacial lakes significantly accelerate the melt of the ice sheet, with the PLISI-induced mass loss being accelerated by the increased surface melt rates over the low-lying lacustrine shelves. Both studies find that the enhanced retreat by proglacial lakes is not caused by calving or basal melting, but rather due to PLISI and the negative surface mass balance. This is because ice shelves have a low surface elevation with high temperatures and strong ablation.

Here, we expand on the work by Hinck et al. (2022) and Quiquet et al. (2021) by using an ice-sheet model that includes both the North American and Eurasian ice sheets on consecutive glacial cycles. Here, we use an ice-sheet model with a hybrid GCM climate forcing to study the effect of proglacial lakes on glacial terminations throughout the Late Pleistocene. Rather than making sea level projections, our main goal is to investigate ice dynamical processes that may have contributed to the melt of the North American and Eurasian ice sheets. Here we investigate the effects of basal sliding, shelf formation, and sub-shelf melting on glacial terminations. We also determined the effect of different GIA response time scales on proglacial lakes and glacial terminations.

2. Methods

2.1 Ice-sheet model

We simulated the Northern Hemisphere ice sheets using the 3-D thermomechanically-coupled ice-sheet model IMAU-ICE version 2.0 (Berends et al., 2022). The hybrid shallow ice / shallow shelf approximation is used to calculate the flow of ice (Bueler and Brown, 2009). To model GIA, we use an Elastic Lithosphere Relaxing Asthenosphere model (ELRA; Le Meur and Huybrechts, 1996). Basal friction is calculated using a Budd-type sliding law (Bueler and van Pelt, 2015). The spatially variable bed roughness needed to calculate basal friction is parameterised following the approach of Martin et al. (2011). Basal friction at the grounding-line is treated by a sub-grid friction-scaling scheme (Berends et al., 2022) and is based on the approach used in the Community Ice Sheet Model (CISM; Leguy et al., 2021) and the Parallel Ice Sheet Model (PISM; Feldmann et al., 2014). Calving is parameterised by a simple thickness threshold scheme, using a threshold thickness of 200 meters. To calculate sub-shelf melt, we use a linear temperature and depth-dependent sub-shelf melt parameterization (Martin et al. 2011). Ocean temperatures are parameterised, with globally uniform ocean temperature changes (De Boer et al., 2013) which do not capture regional variations in ocean temperatures. We apply the same sub-shelf melting method for oceans and proglacial lakes unless stated otherwise. Lakes and ocean are simulated when the bedrock is below the modelled sea level, an approach similar to Quiquet et al. (2021). Hinck et al. (2022), used a lake model that can simulate lake surfaces above sea level. Hinck et al. (2022) showed that retreat is faster with such a lake model rather than the method shown here. Therefore, the effect of proglacial lakes may be underestimated in this study.

The North American, Eurasian and Greenland ice sheets are simulated in three separate domains. North America and Eurasia have a 40 x 40 km spatial resolution and Greenland 20 x 20 km. The boundaries of these domains are shown in Fig. 1.

https://doi.org/10.5194/cp-2023-42
Preprint. Discussion started: 3 July 2023

The higher resolution of the Greenland ice sheet results in a similar number of grid-cell compared to the other two domains, while capturing smaller topographic features. As shown in Fig. 1, the domains have some overlapping regions. Therefore, regions that appear in more than one model domain are only allowed to have ice in one of them; e.g., ice on Ellesmere Island is only simulated in the North American domain but not in the Greenland domain, while ice on Greenland itself is not simulated in the North America domain. We simulate Greenland and North America in separate domains, but they are thought to have merge during glacial periods.

2.2 Climate forcing

To calculate the melt and accumulation of ice, our surface mass balance model (see section 2.4) requires information on precipitation and temperature as a function of time and space. To obtain the climate forcing computationally efficiently we interpolate between pre-calculated pre-industrial (PI) and last glacial maximum (LGM; 21 kyr ago) time-slices using a matrix method (Pollard et al., 2010). This allows us to implicitly include climate – ice-sheet interactions at low computational costs and is a good alternative to fully-coupled ice-climate set-ups, which are currently still unfeasible due to the high computational costs. Details of this method, which is based on Berends et al. (2018) and Scherrenberg et al. (2023), are described in appendix C.

The matrix method includes a precipitation-topography, albedo-temperature, and elevation-temperature feedback to interpolate between the LGM and PI climate time-slices. Precipitation is calculated based on the local and domain-wide change in topography. Therefore, this method implicitly accounts for changes in precipitation resulting from local and large-scale topography changes induced by the ice sheet. Temperature is interpolated with respect to the external forcing and the annual absorbed insolation by the surface, both contributing equally to the interpolation weight in the matrix method. Absorbed insolation is calculated using the ice-sheet model's surface albedo and incoming insolation following the orbital solutions from Laskar et al. (2004). To calculate the annual absorbed insolation index, we interpolate the annual absorbed insolation in the model to reference fields calculated using the LGM and PI climate and the corresponding land and ice masks (Abe-Ouchi et al., 2015). To compute the contribution from external forcing, we use a combination of CO_2 and insolation to calculate the external forcing index. Fig. 2 shows how CO_2 (Fig. 2b) and insolation (Fig. 2c) contribute to the external forcing index (Fig. 2a). Atmospheric CO_2 is obtained from two different sources, depending on the time-period. For the past 800 kyr we use ice-core CO_2 from Bereiter et al. (2015). For time-periods before 800 kyr ago, which we use as a spin-up of our simulation, we use leaf-wax proxy-based CO_2 reconstructions from Yamamoto et al. (2022). They have a good agreement with the ice-core record for the overlapping period. To derive a forcing index from both CO_2 and insolation, we first determine an index for CO_2, where 0 is LGM (190 ppm) and 1 is PI (280 ppm) climate. We then modify this index using the 65°N summer insolation to capture temperature changes caused by the orbital cycles.

With stronger (weaker) summer insolation the index is increased (decreased) and the climate forcing becomes closer to PI (LGM). The forcing index remains unchanged if the insolation is 440 W/m^2 (see Fig. 2a). Finally, the forcing index is capped between -0.25 and 1.25 to prevent too much extrapolation of the forcing. The resulting forcing index is shown in Fig.

https://doi.org/10.5194/cp-2023-42
Preprint. Discussion started: 3 July 2023

2. This figure shows that for LGM CO_2 concentrations, the forcing index can still be relatively high for strong insolation, and the forcing index for PI CO_2 levels can be relatively low for weak insolation values. The forcing index (a function of time) is then combined with the modelled annual absorbed insolation (a function of time and space) to interpolate the PI and LGM temperatures. Preliminary experiments showed that this computationally efficient method of including insolation changes improves the modelled glacial cycles in terms of the timing of deglaciations.

2.3 Climate time-slices and downscaling

When simulating the last glacial cycle using an ice-sheet model, it has been shown that the LGM extent and volume are strongly dependent on the climate forcing (Charbit et al., 2007; Niu et al., 2019, Adler and Hostetler, 2019; Scherrenberg et al., 2023). Not all general circulation models (GCM) can be used to model LGM ice sheet extent that agree well with reconstructions (Scherrenberg et al., 2023). Here we use the mean of MIROC (Sueyoshi et al., 2013), IPSL (Dufresne et al., 2013), COSMOS (Budich et al., 2010) and MPI (Jungclaus et al., 2012) members of the paleoclimate modelling intercomparison project phase 3 (PMIP3; Braconnot et al., 2011). This ensemble has been shown to yield good LGM extent in combination with IMAU-ICE (Scherrenberg et al., 2023). To correct for biases in the GCM data, we calculate the difference between the PI time-slice and the reanalysis from ERA40 (Uppala et al., 2005). This bias is then applied to both the PI and LGM time-slice. However, the resulting PI time-slice may contain some of the anthropogenic warming enclosed in ERA40.

The topography and spatial resolution differ between the climate forcing and the ice-sheet model. Therefore, some corrections need to be applied before the climate forcing can be used in IMAU-ICE. First, we bilinearly interpolate the climate forcing to the finer ice-sheet model grid. As the climate forcing has a lower resolution and therefore a smoother topography, some topographic corrections need to be applied to the temperature and precipitation fields. For temperature, we apply a lapse-rate-based correction. For precipitation we use the Roe and Lindzen (2001) model to capture the orographic forcing of precipitation on the sloping ice margin, and the plateau desert in the ice-sheet interior. A more detailed description of the bias correction and downscaling methods can be found in appendix B.

2.4 Surface mass balance model

The surface mass balance (SMB) is calculated monthly using IMAU-ITM (insolation-temperature model; Berends et al., 2018). For the present-day climate this provides an adequate SMB distribution as shown in the Greenland surface mass balance model intercomparison project (GrSMBMIP; Fettweis et al., 2020). Using this model, accumulation of snow is calculated using the large-scale snow-rain partitioning proposed by Ohmura, (1999). Refreezing is calculated following a scheme by Huybrechts and de Wolde, (1999) and Janssen and Huybrechts, (2000). Ablation is calculated based on Bintanja et al. (2002) and depends on temperature, insolation and albedo. The equations describing IMAU-ITM are discussed in more detail in appendix A.

https://doi.org/10.5194/cp-2023-42
Preprint. Discussion started: 3 July 2023

3. Results

We conduct a spin-up experiment where the model simulates the Northern Hemisphere ice sheets during the period from 1450 kyr ago to 800 kyr ago with CO_2 forcing obtained from leaf-wax proxy data by Yamamoto et al. (2022). We then conduct a "Baseline" experiment by continuing this experiment from 800 kyr ago to present-day with CO_2 forcing obtained from ice cores by Bereiter et al. (2015). The total sea-level contribution of this Baseline is shown in Fig. 3 and compared to ice volume reconstructions by Spratt and Lisiecki (2016), and Grant et al. (2014). Since we only simulate Northern-Hemisphere ice sheets, we added 30% to the ice sheet contribution to account for sea level changes caused by processes other than the Northern-Hemisphere ice sheets, such as the Antarctic and Patagonian ice sheets (Simms et al., 2019). We find that the modelled sea level matches the reconstructions well and our simulation captures all major melting events throughout the Late Pleistocene. The modelled interglacial periods are long compared to reconstructions, which may have resulted from the PI temperatures. Due to a bias correction based on observations our PI time-slice shows some anthropogenic warming. Therefore, ice inception requires relatively low CO_2 concentrations and weak insolation. Nevertheless, the ability of the model to capture the overall pattern of glacial terminations and interglacial periods allows us to study the importance of ice dynamical processes that may have contributed to the decay of the ice sheets.

Fig. 4 shows the total ice volume changes for the Northern Hemisphere (Fig. 4a), North American (Fig. 4c) and Eurasian (Fig. 4e) ice sheets. Blue indicates net accumulation and red indicates net melt of the ice sheets. Red squares have been added to indicate the onset of deglaciations or interstadials. A blue circle is added at the start of glaciations or the end of interstadials. These model states are compared to the external forcing index in Fig. 4b, d and f, where an external forcing index of 0 (1) signifies LGM (PI) climate.

Obviously, when the climate becomes colder (warmer) the ice sheet will tend to have net accumulation (ablation). However, when the ice sheet becomes larger, the climate needs to be colder, or specifically more glacial, to be able to maintain net accumulation. This agrees with Abe-Ouchi et al. (2013) and Parrenin and Paillard (2003) and shows that a larger ice sheet is more vulnerable to a decay. Once the ice sheet reaches LGM volume, any additional cooling barely increases the size of the ice sheet. This may partly result from the precipitation-topography feedback implemented in the model. As the ice sheet becomes larger, the climate becomes more arid and less moisture is available to grow the ice sheet. At the same time the ice sheet size at LGM is somewhat constrained by the fact that large marginal regions border the ocean which prevents further lateral extension.

Furthermore, the Eurasian ice sheet (Fig. 4f) is more sensitive to insolation and CO_2 increases compared to the North American ice sheet (Fig. 4d). The same CO_2 concentrations and insolation can facilitate decay of the Eurasian ice sheet and be favourable enough for the North American ice sheet to survive at the same time. This is in line with Bonelli et al. (2009) and Abe-Ouchi et al. (2013), both finding that the Eurasian ice sheet needs lower CO_2 concentrations and insolation compared to the North American ice sheet. The higher sensitivity of the Eurasian ice sheet also follows from ice volume reconstructions,

https://doi.org/10.5194/cp-2023-42
Preprint. Discussion started: 3 July 2023

Climate of the Past Discussions

such as Gowan et al. (2021), who show that the Eurasian ice sheet lost most of its volume during the MIS3 (60-25 kyr ago) interstadial, while the North American ice sheet continued to survive until the LGM.

3.1 Design of the perturbed experiments

To investigate the effect of proglacial lakes and GIA on the Late Pleistocene terminations, we carry out a set of experiments that are similar to the Baseline, but have one process altered. In the Baseline set-up, our model reproduces the basic features of glacial terminations throughout the Late-Pleistocene. For the sensitivity experiments, we modify the Baseline simulation to investigate the effect of sub-shelf melting, sub-shelf basal friction and GIA on the deglaciation of the Northern Hemisphere ice sheets. Each simulation branches off from the Baseline simulation at 782 kyr ago, which is during an interglacial period when the North American and Eurasian continents were mostly ice-free. In the next few sections, we introduce these perturbation experiments to investigate which processes are important for melting the ice sheets. These experiments are described in paragraphs 3.2-3.5 and summarized in Table 1.

Table 1: A description of the experiments. Each perturbed experiment is similar to the Baseline except for the described feature.

Experiment	Description	Section
Zero BMB	Basal mass balance is set to 0 everywhere	3.2
Rough Water	The basal friction of floating ice is the same as land	3.3
Fast GIA	The GIA relaxation time is decreased from 3,000 to 300 years	3.4
Slow GIA	The GIA relaxation time is increased from 3,000 to 10,000 years	3.4

3.2 The effect of basal melt on glacial cycles

First of all, proglacial lakes facilitate ice shelves, which can undergo sub-shelf melting. Sub-shelf melting is considered an important process for the mass-loss of Antarctica (Pritchard et al., 2012; Shepherd et al., 2018). While sub-shelf melting underneath Antarctica's shelves is dominated by temperature and salinity gradients, Lake Agassiz was a fresh water lake created by the melting ice sheet. Therefore, we conduct a sensitivity test to investigate if sub-shelf melting could have a significant impact on the retreat of the North American and Eurasian ice sheets.

The Zero BMB experiment deviates from the Baseline by setting the sub-shelf melt rate to 0. Fig. 5 shows the ice-volume time-series calculated in the Zero BMB experiment and compares it to the Baseline. Fig. 5b-k show the terminations in more detail. Zero BMB is similar to the Baseline, though the ice sheets during glacial periods are slightly bigger. However, the Zero BMB has only a small effect on the glacial terminations, delaying full deglaciation by up to a few centuries.

https://doi.org/10.5194/cp-2023-42
Preprint. Discussion started: 3 July 2023

3.3 The effect of basal friction of floating ice

The ice shelves floating on proglacial lakes or seas experience negligible basal friction, which results in relatively high flow velocities. To study the impact of this lack of friction, we conduct the Rough Water experiment where the friction coefficient of ocean/lake water is not set to zero, but instead is calculated as if the ice were grounded. This essentially prevents the formation of shelves, so that a migration of the groundling line will not cause a change in friction, which prevents PLISI/MISI. While this is a very unrealistic scenario, the groundling line does not migrate far into the ocean due to strong ablation. The sea level contribution for the Rough Water experiment can also be found in Fig. 5 and is compared to Zero BMB and the Baseline. During the onset of the termination, the Rough Water experiment losses mass at roughly the same pace as the Baseline. However, once more than half of the ice volume is lost, the mass loss rate in Rough Water slows down with respect to the Baseline. This is because the proglacial lakes are only created once the ice sheet has already partly retreated. Therefore, while the Baseline and Rough Water experiments have a similar retreat rate at the onset of the termination, the retreat in the Baseline simulation accelerates once the proglacial lake has formed. Further differences between the Rough Water and Baseline can be seen in Fig. 6a-d, which shows a transect of the North American ice sheet at 11 kyr ago. While the Baseline simulation has large ice shelves in North America, almost the entire ice sheet is grounded in the Rough Water simulation. The shelves in the Baseline have large ice velocities due to the negligible sub-shelf friction. Consequentially, the surfaces of the ice shelves in the Baseline simulation are flat and close to sea level and therefore experience high temperatures and strongly negative SMB. In the Rough Water simulation, these shelves are very small, and the higher elevation of the grounded ice results in a smaller ablation area.

Fig. 7 compares the forcing index and ice volume for the Rough Water simulation. For North America, the threshold for melt is very similar to the Baseline simulation. However, the Eurasian ice sheet does not fully melt during the Rough Water experiment. Instead, the ice-dome in the Barents-Kara Sea region persist throughout the entire Late Pleistocene, suggesting that MISI may be an important process to melting this ice-dome. Currently, this region is a shallow sea, surrounded by islands such as Novaya Zemlya and Svalbard that have cold enough climates to be partly covered by glaciers. With the high albedo of the Barents-Kara ice dome facilitating lower temperatures, and without the effect of MISI, the ice dome may survive insolation and CO_2 maxima.

3.4 Glacial isostatic adjustment

Proglacial lakes are created by the interaction between GIA, ice sheets and melt water. The large mass of the ice sheet causes a depression in the landscape. As the ice sheet retreats, this depression can facilitate a proglacial lake at the ice margin. The relaxation time of the GIA controls how fast the bedrock fully recovers from a change in ice load. This relaxation time, as well as the thickness of the ice sheet and the retreat rate, may control the size and shape of the proglacial lake. Here we assess the effect of GIA by comparing three simulations; the previously shown Baseline simulation (3000-yr), the Slow GIA (10,000-yr), and Fast GIA (300-yr relaxation time).

https://doi.org/10.5194/cp-2023-42
Preprint. Discussion started: 3 July 2023

Fig. 8 shows the ice volume time-series of these three simulations, with the smaller panels zooming in on individual terminations (Fig. 8b-8k). The retreat in the Slow GIA simulation is up to a millennium slower compared to the Baseline simulation. As the ice sheet grows, the bedrock subsides. However, in the Slow GIA, the subsidence rate is smaller compared to the Baseline. Therefore, at the start of the termination the bedrock in the Slow GIA is further from equilibrium resulting in higher ice and bedrock topography. Therefore, as the ice sheet starts to retreat the SMB is higher leading to a slower deglaciation. However, if the bedrock topography during a glacial maximum is similar to the Baseline, the retreat will be similar as well (see Fig. 8j). Slow GIA also has a delayed inception phase (see Fig. 8a). Due to the slow bedrock uplift, large parts of North America are still below sea level millennia after the ice sheet have fully receded. As a result, regions such as North-Eastern Canada, a location for ice inception, are still below sea level throughout the entire preceding interglacial period.

Fast GIA has a slower deglaciation compared to the Baseline, Slow GIA, and Rough Water simulation, which can be seen in transects shown in Fig. 6. Though, on the contrary to Rough Water, the Eurasian ice sheet can fully melt as MISI is possible in the Barents-Kara Sea region. The delayed deglaciation is due to two processes. Firstly, as the ice sheet retreats, the rapid bedrock rebound quickly eliminates the depression that was left by the ice sheet, preventing the formation of proglacial lakes. Secondly, the ice thickness loss is more efficiently compensated by the bedrock rebound, reducing the elevation-temperature feedback and thereby reducing surface melt rates. The combination of the lack of lakes and the SMB-elevation feedback makes the Fast GIA the simulation with the slowest melt shown here.

4. Discussion

In this study, we investigate the effect of proglacial lakes on the deglaciation of the Eurasian and North American ice sheets throughout the past 800 kyr. In the Baseline configuration, the modelled ice volume over time generally agrees well with different sea-level reconstructions, so that all major deglaciations throughout the Late Pleistocene are captured. However, a shortcoming is that our simulations tend to have slightly too long interglacial periods compared to reconstructions, especially MIS-11 interglacial which had higher global temperatures and sea-levels compared to present day (Hearty et al., 1999; Raymo and Mitrovica, 2012). Sea levels that are higher than 7.4 meters with respect to present day are not possible as we do not model the Antarctic ice sheet. Warmer than pre-industrial temperatures are also not captured, as our climate forcing was interpolated from PI and LGM time-slices. Therefore, any climate that has both higher CO_2 concentrations and summer insolation than PI will require some extrapolation. Adding additional time-slices to our matrix method, similar to Abe-Ouchi et al. (2013), may improve our representation of different ice volume, CO_2 concentration and orbital parameters. However, as shown by Scherrenberg et al. (2023), the ice sheet extent depends strongly on the climate forcing. Here we have chosen a forcing that would result in an LGM extent that agrees well with reconstructions rather than a large number of time-slices.

The matrix method, which we use to interpolate between the LGM and PI time-slices, implicitly includes a temperature-albedo and precipitation-topography feedback. However, ice-sheet climate interactions can exhibit threshold behaviours which cannot be simulated using our method. For example, the opening and closing of straits such as the Canadian

https://doi.org/10.5194/cp-2023-42
Preprint. Discussion started: 3 July 2023

Arctic Archipelago (Löfverström et al., 2022) or the response of Heinrich and Dansgaard/Oeschger events (Claussen et al., 2003), or rapid changes in ocean circulation and sea ice due to the influx of melt water into the ocean (Otto-Bliesner and Brady, 2010). Additionally, since we do not model the ocean, there is no interactions between melt water and ocean circulation. Including many of these threshold behaviours would require a model that more explicitly simulates the climate system. GCM models may be able to simulate these interactions, but simulating glacial cycles is unfeasible as it requires a too large amount of computational resources. Though, ocean-atmosphere circulation models can be used to simulate individual glacial terminations (Obase et al., 2021). Alternatively, intermediate complexity models (Ganopolski and Calov., 2011) can more explicitly calculate feedbacks in the climate system, though still at high computational costs and with more parameterizations compared to full GCMs.

5. Conclusion

We have studied the relative importance of different ice-dynamical processes for glacial terminations. The onset of terminations is dominated by a decrease in SMB, which induces retreat of the ice sheet. The Eurasian ice sheet is more sensitive to higher CO_2 concentrations and insolation compared to North America, and will therefore retreat more often. Once the ice sheets have retreated significantly, proglacial lakes are created at the margin of the ice sheets. Our results show that proglacial lakes can significantly accelerate the collapse of the North American and Eurasian ice sheets. If these lakes are not present, North America and Eurasia deglaciate at a reduced pace, and often remain partially ice-covered.

The largest impact of proglacial lakes is caused by the low friction of floating ice. If the basal friction of shelves is the same as grounded ice, which removes the effect of PLISI and MISI, the Eurasian ice sheet does not fully melt and an ice-dome persists in the Barents-Kara Sea throughout the interglacial. While the North American ice sheet does eventually disappear, removing the lakes delays this by a few millennia. This is in line with Hinck et al. (2022) and Quinquet et al. (2021), who suggested that PLISI has a large impact on the melt of the North American ice sheet. We find that this is mainly due to the elevation-temperature feedback, where the high flow velocities of shelves cause them to thin. The resulting lower surface elevations result in increased surface melt.

We found that sub-shelf melting is only a secondary effect to the mass loss of the ice sheets. Applying a zero sub-shelf melt rate still results in a full deglaciation, although it may take a few additional centuries to complete. Applying a more sophisticated sub-shelf melting scheme in the Baseline experiment, to simulate high melt rates near the grounding line (Rignot and Jacobs, 2002), may result in a more substantial impact from sub-shelf melting. Nevertheless, this smaller impact of sub-shelf melting is in line with both Hinck et al. (2022) and Quinquet et al. (2021). Additionally, since proglacial lakes consist of fresh water, it is doubtful whether such high melt rates, which at present are a result of salinity-driven overturning, should be expected at all.

The size and shape of proglacial lakes follow from the interaction between GIA and ice thickness. Here we have used uniform GIA response times, but in reality, GIA varies spatially (e.g., Forte et al., 2010) and have large uncertainties. If the

https://doi.org/10.5194/cp-2023-42
Preprint. Discussion started: 3 July 2023

Climate of the Past
Discussions

GIA responds slower compared to our Baseline, the termination will be up to a millennium slower and the subsequent inception phase is delayed. Since the inception sites are typically also the last regions to deglaciate, the land can still be below sea level at the onset of the next glacial period only if the bedrock rebound is too slow. We find that a GIA response that is substantially faster than the Baseline has a slower deglaciation. The North American ice sheet may not even fully deglaciate during some interglacial periods. This is because proglacial lakes are not created when the bedrock uplift is too fast. Additionally, surface melt is reduced as the bedrock uplift more efficiently compensates the thickness loss.

The importance of understanding marine ice-sheet dynamics and ice-sheet climate interactions when projecting the future mass loss of the Greenland and Antarctic ice sheets is well known. Our results underline the fact that these processes are just as relevant for understanding past ice-sheet evolution, so that reproducing this evolution can help constrain these processes.

Appendix A: Surface mass balance model

The surface mass balance (SMB) is calculated using an insolation-temperature model; IMAU-ITM (Berends et al., 2018). To calculate the SMB, ice is added due to snow and refreezing and is removed due to melt. To calculate accumulation and ablation of ice, the model requires temperature and precipitation fields, which were obtained from downscaled and bias-corrected GCM output (see appendix B and C). To calculate the amount of snowfall, we apply a temperature-based snow-rain partitioning with respect to the melting point ($T0$) by Ohmura et al. (1999).

$$f_{snow} = 0.5\left(1 - \frac{\operatorname{atan}\frac{(T(x,y,m)-T0)}{3.5}}{1.25664}\right). \tag{1}$$

The snow fraction (f_{snow}) determines the amount of precipitation that falls as snow; the remainder falls as rain. x and y indicate the horizontal grid while m indicates the month. To calculate the ablation of ice, we use the parameterised scheme by Bintanja et al. (2002) that accounts for ablation from temperature and insolation:

$$Melt(x,y,m) = (c_1\,(T(x,y,m) - T_0) + c_2\,(1 - \alpha(x,y,m))\,Q_{TOA}(x,y,m) - c_3). \tag{2}$$

Here, T is the 2-meter air temperature, T_0 is the melting temperature of ice or 273.15 K, Q_{TOA} is the insolation at the top of the atmosphere (Laskar et al., 2004). The parameters for c_1, c_2 are 0.079 m/yr/K and 7.9×10^{-4} m/J. The parameter c_3 is used for tuning. Here we have tuned the model to obtain realistic LGM ice volumes, with c_3 values for North America (-0.28 m/yr) Eurasia (-0.24 m/yr) and Greenland (0.19 m/yr). Albedo (α) is calculated in the ice-sheet model and is also based on Bintanja et al. (2002):

$$\alpha_{surface}(x,y,m) = \alpha_{snow} - (\alpha_{snow} - \alpha_{background})\mathrm{e}^{-15\,D_{firn}(x,y,m-1)} - 0.015\,Melt_{prev}(x,y). \tag{3}$$

The $\alpha_{background}$ represents the albedo without any snow, with 0.5 for bare ice, 0.2 for land and 0.1 for water. Melt of the previous year is defined as $Melt_{prev}$. If snow is added on top, which increases the firn depth (D_{firn}), the albedo can increase until α_{snow}, which represents the albedo of fresh snow (0.85). Therefore, the albedo in the model varies between the

https://doi.org/10.5194/cp-2023-42
Preprint. Discussion started: 3 July 2023

background and snow albedo. The depth of the firn layer is calculated using the amount of snow that is added on top without melting.

Some of the melt and rainfall can refreeze in the model. Here we use the approach by Huybrechts and de Wolde (1999), using the total amount of liquid water (L), superimposed water (S) and precipitation (P).

$$S(x,y,m) = \max\{0, 0.012(T0 - T(x,y,m))\}. \tag{4}$$

$$L(x,y,m) = Rain(x,y,m) + Melt(x,y,m). \tag{5}$$

$$Refreezing(x,y,m) = \min\{\min\{S(x,y,m), L(x,y,m)\}, P(x,y,m)\}. \tag{6}$$

By combining the snowfall, refreezing and melt the SMB can be calculated:

$$SMB(x,y,m) = Snow(x,y,m) + Refreezing(x,y,m) - Melt(x,y,m). \tag{7}$$

Appendix B: Downscaling and bias correction

To account for differences between the general circulation model (GCM) simulations and observed climate (ERA40; Uppala et al., 2005), we apply a bias correction on both the LGM and PI snapshots.

To account for the temperature bias, we first have to scale the temperature to sea level using a lapse-rate correction. This is to account for differences in topography between the GCM and ERA40 data.

$$T_{obs,SL}(x,y,m) = T_{obs,PD}(x,y,m) + Hs_{obs,PD}(x,y)\,\lambda(x,y). \tag{8}$$

$$T_{GCM,SL}(x,y,m) = T_{GCM,PI}(x,y,m) + Hs_{GCM,PI}(x,y)\,\lambda(x,y). \tag{9}$$

Here, T is the temperature from ERA40 (obs) and the climate model (GCM). Surface height is defined as Hs_{GCM}. The temperature lapse rate is represented by λ. Once the temperature is applied to sea level (SL), we calculate the temperature difference between the climate model and observed climate:

$$T_{GCM,bias}(x,y,m) = T_{GCM,SL}(x,y,m) - T_{obs,SL}(x,y,m). \tag{10}$$

This bias correction is then subtracted from the PI and LGM snapshots. As a result, the PI snapshot will be the equal to ERA40, which contains some anthropogenic warming.

For precipitation, biases are applied as ratios rather than absolute differences, to ensure that the bias-corrected values are always positive. Therefore, we use the ratio between the model and observed fields instead:

$$P_{GCM,bias}(x,y,m) = P_{GCM,PI}(x,y,m) \,/\, P_{obs,PI}(x,y,m). \tag{11}$$

This ratio is used to calculate the bias corrected precipitation for PI and LGM:

$$P_{GCM,corr}(x,y,m) = P_{GCM}(x,y,m) \,/\, P_{GCM,bias}(x,y,m). \tag{12}$$

Appendix C: Climate time-slice interpolation

To provide the ice-sheet model with transiently changing forcing using minimal computational resources, we interpolate between pre-calculated LGM and PI climate time-slices. To interpolate the time-slices we have used a matrix method. Our

https://doi.org/10.5194/cp-2023-42
Preprint. Discussion started: 3 July 2023

approach is based on Berends et al. (2018) and Scherrenberg et al. (2023) and uses different methods for temperature and precipitation.

To calculate the temperature forcing, we use a linear interpolation:

$$T_{mod}(x,y,m) = w_{tot,T}(x,y)\, T_{PI,corr}(x,y,m) + \left(1 - w_{tot,T}(x,y)\right) T_{LGM,corr}(x,y,m). \quad (13)$$

Here, T_{mod} is the temperature forcing in the ice sheet model. $T_{PI,corr}$ and $T_{LGM,corr}$ are the climate model temperatures for PI and LGM respectively. w_{tot} is the interpolation weight and depends on two processes: the external forcing (w_{ext}) and an albedo feedback (w_{ice}). For North America and Eurasia, w_{tot} is calculated as following:

$$w_{tot,T}(x,y) = \frac{(w_{ext}(x,y) + w_{ice}(x,y))}{2}\ . \quad (14)$$

In Greenland the albedo changes almost exclusively due to the change in ice-sheet extent. Our model does not include sea ice and the Greenland domain does not contain extensive tundra areas. Therefore, we apply a smaller contribution from albedo in this domain:

$$w_{tot,T}(x,y) = \frac{(3\, w_{ext}(x,y) + w_{ice}(x,y))}{4}. \quad (15)$$

To calculate w_{ext} we combine the effect of CO_2 (ppm; Bereiter et al., 2015) and insolation at 65°N (W/m^2; Laskar et al., 2004):

$$w_{ext} = \frac{CO2 - CO2_{LGM}}{CO2_{PI} - CO2_{LGM}} + \frac{QTOA_{65°N} - 440}{70}. \quad (16)$$

In this equation, $CO2_{PI}$ and $CO2_{LGM}$ are 190 and 280 ppm respectively. By including the summer (June, July, August) insolation at 65°N ($QTOA_{65°N}$), the climate can become colder or warmer even if the CO_2 concentration is constant (see Fig. 1).

To calculate w_{ice}, which represents an albedo feedback, we calculate the annual absorbed insolation. The absorbed insolation (I_{abs}) depends on the monthly internally calculated albedo ($\alpha_{surface}$) and insolation at the top of the atmosphere (Q_{TOA}):

$$I_{abs}(x,y) = \sum_{m=1}^{12} Q_{TOA}(x,y,m)\, \left(1 - \alpha_{surface}(x,y,m)\right). \quad (17)$$

The albedo is calculated in the ice-sheet model using Eq. 3. To calculate an interpolation weight, from the absorbed insolation (w_{ins}), we need to calculate reference fields for the LGM and PI. To calculate the albedo for these time-slices, we use land and ice masks from the ice sheet reconstruction by Abe-Ouchi et al. (2015) as these were also used in the climate model simulations. We integrate the SMB model forward through time with a fixed climate and ice-sheet geometry until the firn layer reaches a steady state (typically after ~30 years). We can then use Eq. 17 to calculate the reference fields for absorbed insolation. These absorbed insolation fields can then be used to calculate w_{ins}.

$$w_{ins}(x,y) = (I_{abs}(x,y) - I_{abs,LGM}(x,y))\ /\ (I_{abs,PI}(x,y) - I_{abs,LGM}(x,y))\ . \quad (18)$$

To account for both the local and domain wide change in albedo and insolation, we use the following equation:

$$w_{ice}(x,y) = \frac{w_{ins}(x,y) + 3\, w_{ins,smooth}(x,y) + 3\, w_{ins,av}(x,y)}{7}. \quad (19)$$

https://doi.org/10.5194/cp-2023-42
Preprint. Discussion started: 3 July 2023

Climate of the Past Discussions

Here, $w_{ins,av}$ is the domain-wide averaged interpolation weight and w_{ins} is the local interpolation weight. $w_{ins,smooth}$ represents the regional temperature effect and is calculated by applying a 200 km gaussian smoothing on w_{ins}. Once again, we use a slightly different method for Greenland due to the lack of tundra regions:

$$w_{ice}(x,y) = \frac{w_{ins,smooth}(x,y) + 6\, w_{ins,av}}{7}. \tag{20}$$

The interpolation weight to calculate temperature ($w_{tot,T}$) can now be derived from w_{ice} and w_{ext} using Eq. 14 or 15. This interpolation weight will change depending on albedo, insolation and CO_2.

For precipitation, we apply a slightly different method, as the precipitation does not change linearly when the climate cools down and topography changes. We use the following equation to interpolate the precipitation from the climate time-slices:

$$P_{ref} = e\left((1 - w_{LGM}(x,y))\log\left(P_{PI,corr}(x,y,m)\right) + w_{LGM}(x,y)\log\left(P_{LGM,corr}(x,y,m)\right)\right). \tag{21}$$

w_{LGM} is the interpolation weight and depends on local and domain-wide topography changes. First, we compare the domain-wide topography in the model to the climate time-slices using the following equation:

$$w_{tot,P} = \left(\sum Hs\,(x,y) - \sum Hs_{PI}(x,y)\right) / \left(\sum Hs_{LGM}(x,y) - \sum Hs_{PI}(x,y)\right). \tag{22}$$

The surface topography is represented by Hs. $w_{tot,P}$ represents the interpolation weight from the domain-wide change in topography. If a grid-cell was covered with ice during the LGM, we also interpolate with respect to local changes in topography:

$$w_{LGM,Hs}(x,y) = \frac{Hs_{ISM}(x,y) - Hs_{GCM\,PI}(x,y)}{Hs_{GCM,LGM}(x,y) - Hs_{GCM,PI}(x,y)}\, w_{tot,P}(x,y). \tag{23}$$

If a grid-cell did not have ice during the LGM, $w_{LGM,Hs}$ is equal to $w_{tot,P}$. In the last step, we multiply the local and regional precipitation effect to obtain the interpolation weight for precipitation:

$$w_{LGM}(x,y) = w_{LGM,Hs}(x,y)\, w_{tot,P}(x,y). \tag{24}$$

The resulting w_{LGM} from Eq. 24 is used in Eq. 20 to calculate the precipitation forcing.

Code availability: The source code for IMAU-ICE can be found at https://github.com/IMAU-paleo/IMAU-ICE. The version used in this study as well as the configuration files are available at Zenodo [DOI will be added upon acceptation]. To run the simulations additional files are required for CO_2, climate and initial topography. For more information, contact the corresponding author.

Data availability: The results are available in a 5 kyr (2D fields) and 100-year (scalar) output frequency at Zenodo [DOI will be added upon acceptation]. Additional 2D fields and higher output frequencies up to 1 kyr can be requested by contacting the corresponding author.

Author contributions. MS conducted the simulations and has written the manuscript. The set-up for the experiments was created by RW, CB and MS. CB provided model support. All authors have provided input to the manuscript and analysis of the results.

Competing interest. The authors declare that they have no conflict of interest

Acknowledgements. M.D.W. Scherrenberg is supported by the Netherlands Earth System Science Centre (NESSC), which is financially supported by the Ministry of Education, Culture and Science (OCW) on grant no. 024.002.001. C.J. Berends is funded by PROTECT. This project has received funding from the European Union's Horizon 2020 research and innovation programme under grant agreement No 869304, PROTECT contribution number [will be assigned upon publication]. The Dutch Research Council (NWO) Exact and Natural Sciences supported the supercomputer facilities for the Dutch National Supercomputer Snellius. We would like to acknowledge the support of SurfSara Computing and Networking Services.

References

Abe-Ouchi, A., Saito, F., Kawamura, K., Raymo, M. E., Okuno, J., Takahashi, K., and Blatter, H.: Insolation-driven 100,000-year glacial cycles and hysteresis of ice-sheet volume, Nature, 500, 190–193, https://doi.org/10.1038/nature12374, 2013.

Abe-Ouchi, A., Saito, F., Kageyama, M., Braconnot, P., Harrison, S. P., Lambeck, K., Otto-Bliesner, B. L., Peltier, W. R., Tarasov, L., Peterschmitt, J.-Y., and Takahashi, K.: Ice-sheet configuration in the CMIP5/PMIP3 Last Glacial Maximum experiments, Geosci. Model Dev., 8, 3621–3637, https://doi.org/10.5194/gmd-8-3621- 2015, 2015.

Alder, J. R. and Hostetler, S. W.: Applying the Community Ice Sheet Model to evaluate PMIP3 LGM climatologies over the North American ice sheets, Clim. Dynam., 53, 2807–2824, https://doi.org/10.1007/s00382-019-04663-x, 2019.

Annan, J. D., Hargreaves, J. C., and Mauritsen, T.: A new global surface temperature reconstruction for the Last Glacial Maximum, Clim. Past, 18, 1883–1896, https://doi.org/10.5194/cp-18-1883-2022, 2022

Batchelor, C. L., Margold, M., Krapp, M., Murton, D., Dalton, A. S., Gibbard, P. L., Stokes, C. R., Murton, J. B., and Manica, A.: The configuration of Northern Hemisphere ice sheets through the Quaternary, Nat. Commun., 10, 3713, https://doi.org/10.1038/s41467-019-11601-2, 2019.

Bereiter, B., Eggleston, S., Schmitt, J., Nehrbass-Ahles, C., Stocker, T. F., Fischer, H., Kipfstuhl, S., and Chappellaz, J.: Revision of the EPICA Dome C CO2 record from 800 to 600kyr before present, Geophys. Res. Lett., 42, 542–549, https://doi.org/10.1002/2014GL061957, 2015.

https://doi.org/10.5194/cp-2023-42
Preprint. Discussion started: 3 July 2023

Berends, C. J., de Boer, B., and van de Wal, R. S. W.: Application of HadCM3@Bristolv1.0 simulations of paleoclimate as forcing for an ice-sheet model, ANICE2.1: set-up and benchmark experiments, Geosci. Model Dev., 11, 4657–4675, https://doi.org/10.5194/gmd-11-4657-2018, 2018.

Berends, C. J., Köhler, P., Lourens, L. J., and van de Wal, R. S. W.: On the cause of the mid-Pleistocene transition, Rev. Geophys., 59, e2020RG000727, https://doi.org/10.1029/2020RG000727, 2021.

Berends, C. J., Goelzer, H., Reerink, T. J., Stap, L. B., and van de Wal, R. S. W.: Benchmarking the vertically integrated ice-sheet model IMAU-ICE (version 2.0), Geosci. Model Dev., 15, 5667–5688, https://doi.org/10.5194/gmd-15-5667-2022, 2022.

Bintanja, R., van de Wal, R. S. W., and Oerlemans, J.: Global ice volume variations through the last glacial cycle simulated by a 3-D ice dynamical model, Quatern. Int., 95–96, 11–23, 2002.

Bonelli, S., Charbit, S., Kageyama, M., Woillez, M.-N., Ramstein, G., Dumas, C., and Quiquet, A.: Investigating the evolution of major Northern Hemisphere ice sheets during the last glacial-interglacial cycle, Clim. Past, 5, 329–345, https://doi.org/10.5194/cp-5-329-2009, 2009.

Braconnot, P., Harrison, S. P., Otto-Bliesner, B. L., Abe-Ouchi, A., Jungclaus, J. H., and Peterschmitt, J.-Y.: The Paleoclimate Modeling Intercomparison Project contribution to CMIP5, CLIVAR Exchanges, 56, 15–19, 2011.

Budich, R., Gioretta, M., Jungclaus, J., Redler, R., and Reick, C.: The MPI-M Millennium Earth System Model: An assembling guide for the COSMOS configuration, Tech. rep., Max-Planck Institute for Meteorology, Hamburg, Germany, https://pure.mpg. de/rest/items/item_2193290/component/file_2193291/content (last access: 2 February 2023), 2010.

Bueler, E. and Brown, J.: The shallow shelf approximation as a sliding law in a thermomechanically coupled ice sheet model, J. Geophys. Res., 114, F03008, https://doi.org/10.1029/2008JF001179, 2009.

Bueler, E. and van Pelt, W.: Mass-conserving subglacial hydrology in the Parallel Ice Sheet Model version 0.6, Geosci. Model Dev., 8, 1613–1635, https://doi.org/10.5194/gmd-8-1613-2015, 2015.

Charbit, S., Ritz, C., Philippon, G., Peyaud, V., and Kageyama, M.: Numerical reconstructions of the Northern Hemisphere ice sheets through the last glacial-interglacial cycle, Clim. Past, 3, 15–37, https://doi.org/10.5194/cp-3-15-2007, 2007.

Clark, P. U. and Tarasov, L.: Closing the sea level budget at the Last Glacial Maximum, P. Natl. Acad. Sci., 111, 15861–15862, https://doi.org/10.1073/pnas.1418970111, 2014.

Claussen, M., Ganopolski, A., Brovkin, V., Gerstengarbe, F.-W., and, Werner, P.: Simulated global-scale response of the climate system to Dansgaard/Oeschger and Heinrich events, Clim. Dynam., 21, 361–370, https://doi.org/10.1007/s00382-003-0336-2, 2003.

de Boer, B., van de Wal, R., Lourens, L. J., Bintanja, R., and Reerink, T. J.: A continuous simulation of global ice volume over the past 1 million years with 3-D ice-sheet models, Clim. Dynam., 41, 1365–1384, 2013.

Denton, G. H., Anderson, R. F., Toggweiler, J., Edwards, R., Schaefer, J., and Putnam, A.: The last glacial termination, Science, 328, 1652–1656, https://doi.org/10.1126/science.1184119, 2010. Dufresne, J.-L., Foujols, M.-A., Denvil, S., Caubel, A., Marti, O., Aumont, O., Balkanski, Y., Bekki, S., Bellenger, H., Benshila, R., Bony, S., Bopp, L., Braconnot, P.,

https://doi.org/10.5194/cp-2023-42
Preprint. Discussion started: 3 July 2023

Climate of the Past
Discussions
Open Access

Brockmann, P., Cadule, P., Cheruy, F., Codron, F. F., Cozic, A., Cugnet, D., de Noblet, N., Duvel, J.-P., Ethé, C., Fairhead, L., Fichefet, T., Flavoni, S., Friedlingstein, P., Grandpeix, J.-Y., Guez, L., Guilyardi, E., Hauglustaine, D., Hourdin, F., Idelkadi, A., Ghattas, J., Joussaume, S., Kageyama, M., Krinner, G., Labetoulle, S., Lahellec, A., Lefèbvre, M.-P., Lefèvre, F., Lévy, C., Li, Z. X., Lloyd, J., Lott, F., Madec, G., Mancip, M., Marchand, M., Masson, S., Meurdesoif, Y., Mignot, J., Musat, I., Parouty, S., Polcher, J., Rio, C., Schulz, M., Swingedouw, D., Szopa, S., Talandier, C., Terray, P., and Viovy, N.: Climate change projections using the IPSL-CM5 Earth System Model: from CMIP3 to CMIP5, Clim. Dynam., 40, 2123–2165, https://doi.org/10.1007/s00382-012-1636-1, 2013.

Dufresne, J.-L., Foujols, M.-A., Denvil, S., Caubel, A., Marti, O., Aumont, O., Balkanski, Y., Bekki, S., Bellenger, H., Benshila, R., Bony, S., Bopp, L., Braconnot, P., Brockmann, P., Cadule, P., Cheruy, F., Codron, F. F., Cozic, A., Cugnet, D., de Noblet, N., Duvel, J.-P., Ethé, C., Fairhead, L., Fichefet, T., Flavoni, S., Friedlingstein, P., Grandpeix, J.-Y., Guez, L., Guilyardi, E., Hauglustaine, D., Hourdin, F., Idelkadi, A., Ghattas, J., Joussaume, S., Kageyama, M., Krinner, G., Labetoulle, S., Lahellec, A., Lefèbvre, M.-P., Lefèvre, F., Lévy, C., Li, Z. X., Lloyd, J., Lott, F., Madec, G., Mancip, M., Marchand, M., Masson, S., Meurdesoif, Y., Mignot, J., Musat, I., Parouty, S., Polcher, J., Rio, C., Schulz, M., Swingedouw, D., Szopa, S., Talandier, C., Terray, P., and Viovy, N.: Climate change projections using the IPSL-CM5 Earth System Model: from CMIP3 to CMIP5, Clim. Dynam., 40, 2123–2165, https://doi.org/10.1007/s00382-012-1636-1, 2013.

Feldmann, J., Albrecht, T., Khroulev, C., Pattyn, F., and Levermann, A.: Resolution-dependent performance of grounding line motion in a shallow model compared with a full-Stokes model according to the MISMIP3d intercomparison, J. Glaciol., 60, 353–359, https://doi.org/10.3189/2014JoG13J093, 2014.

Fettweis, X., Hofer, S., Krebs-Kanzow, U., Amory, C., Aoki, T., Berends, C. J., Born, A., Box, J. E., Delhasse, A., Fujita, K., Gierz, P., Goelzer, H., Hanna, E., Hashimoto, A., Huybrechts, P., Kapsch, M.-L., King, M. D., Kittel, C., Lang, C., Langen, P. L., Lenaerts, J. T. M., Liston, G. E., Lohmann, G., Mernild, S. H., Mikolajewicz, U., Modali, K., Mottram, R. H., Niwano, M., Noël, B. P. Y., Ryan, J. C., Smith, A., Streffing, J., Tedesco, M., van de Berg, W. J., van den Broeke, M. R., van de Wal, R. S. W., van Kampenhout, L., Wilton, D., Wouters, B., Ziemen, F., and Zolles, T.: GrSMBMIP: intercomparison of the modelled 1980-2012 surface mass balance over the Greenland Ice Sheet, The Cryosphere 14, 3935-3958, https://doi.org/10.5194/tc-14-3935-2020, 2020.

Forte, A., Moucha, R., Simmons, N. A., Grand, S. P., and Mitro- vica, J. X.: Deep-mantle contributions to the surface dynamics of the North American continent, Tectonophysics, 481, 3–15, https://doi.org/10.1016/j.tecto.2009.06.010, 2010.

Ganopolski, A. and Calov, R.: The role of orbital forcing, carbon dioxide and regolith in 100 kyr glacial cycles, Clim. Past, 7, 1415–1425, https://doi.org/10.5194/cp-7-1415-2011, 2011.

Gowan, E. J., Zhang, X., Khosravi, S., Rovere, A., Stocchi, P., Hughes, A. L. C., Gyllencreutz, R., Mangerud, J., Svendsen, J.- 655 I., and Lohmann, G.: A new global ice sheet reconstruction for the past 80 000 years, Nature Communications, 12, 1199, https://doi.org/10.1038/s41467-021-21469-w, 2021.

Grant, K. M., Rohling, E. J., Bronk Ramsey, C., Cheng, H., Edwards, R. L., Florindo, F., Heslop, D., Marra, F., Roberts, A. P., Tamisiea, M. E., and Williams, F.: Sea-level variability over five glacial cycles, Nature Communications, 5, 5076, https://doi.org/10.1038/ncomms6076, 2014.

Hasenfratz, A. P., Jaccard, S. L., Martínez-García, A., Sigman, D. M., Hodell, D. A., Vance, D., Bernasconi, S. M., Kleiven, H. F., Haumann, F. A., and Haug, G. H.: The residence time of Southern Ocean surface waters and the 100 000-year ice age cycle, Science, 363, 1080–1084, https://doi.org/10.1126/science.aat7067, 2019.

Hearty, P. J., Kindler, P., Cheng, H., and Edwards, R. L.: A +20 m middle Pleistocene sea-level highstand (Bermuda and the Bahamas) due to partial collapse of Antarctic ice, Geology, 27, 375–378, https://doi.org/10.1130/0091-7613(1999)027<0375:AMMPSL>2.3.CO;2, 1999.

Hinck, S., Gowan, E. J., Zhang, X., and Lohmann, G.: PISM-LakeCC: Implementing an adaptive proglacial lake boundary in an ice sheet model, The Cryosphere, 16, 941–965, https://doi.org/10.5194/tc-16-941-2022, 2022.

Huybrechts, P. and de Wolde, J.: The dynamic response of the Greenland and Antarctic ice sheets to multiple-century climatic warming, J. Climate, 1, 2169–2188, 1999.

Janssens, I. and Huybrechts, P.: The treatment of meltwater retention in mass-balance parameterizations of the Greenland ice sheet, in: Ann. Glaciol., 31, 2000, edited by: Steffen, K., Ann. Glaciol., Int Glaciological Soc, Cambridge, 133–140, 2000.

Jungclaus, J., Giorgetta, M., Reick, C., Legutke, S., Brovkin, V., Crueger, T., Esch, M., Fieg, K., Fischer, N., Glushak, K., Gayler, V., Haak, H., Hollweg, H.-D., Kinne, S., Kornblueh, L., Matei, D., Mauritsen, T., Mikolajewicz, U., Müller, W., Notz, D., Pohlmann, T., Raddatz, T., Rast, S., Roeckner, E., Salzmann, M., Schmidt, H., Schnur, R., Segschneider, J., Six, K., Stockhause, M., Wegner, J., Widmann, H., Wieners, K.-H., Claussen, M., Marotzke, J., and Stevens, B.: CMIP5 simulations of the Max Planck Institute for Meteorology (MPI-M) based on the MPI- ESM-P model: The lgm experiment, served by ESGF, WDCC at DKRZ, https://doi.org/10.1594/WDCC/CMIP5.MXEPlg, 2012.

Ladant, J.-B., Donnadieu, Y., Lefebvre, V., and Dumas, C.: The respective role of atmospheric carbon dioxide and orbital parameters on ice sheet evolution at the Eocene-Oligocene transition, Paleoceanography, 29, 810–823, https://doi.org/10.1002/2013PA002593, 2014.

Lambeck, K., Rouby, H., Purcell, A., Sun, Y., and Sambridge, M.: Sea level and global ice volumes from the Last Glacial Maximum to the Holocene, P. Natl. Acad. Sci. USA, 111, 15296–15303, https://doi.org/10.1073/pnas.1411762111, 2014.

Laskar, J., Robutel, P., Joutel, F., Gastineau, M., Correia, A. C. M., and Levrard, B.: A long-term numerical solution for the insolation quantities of the Earth, Astron. Astrophys., 428, 261–285, https://doi.org/10.1051/0004-6361:20041335, 2004.

Leguy, G. R., Lipscomb, W. H., and Asay-Davis, X. S.: Marine ice sheet experiments with the Community Ice Sheet Model, The Cryosphere, 15, 3229–3253, https://doi.org/10.5194/tc-15-3229- 2021, 2021.

LeMeur, E. and Huybrechts, P.: A comparison of different ways of dealing with isostasy: examples from modeling the Antarctic ice sheet during the last glacial cycle, Ann. Glaciol., 23, 309–317, https://doi.org/10.3189/S0260305500013586, 1996.

Lepper, K., Buell, A. W., Fisher, T. G., and Lowell, T. V.: A chronology for glacial Lake Agassiz shorelines along Upham's namesake transect, Quaternary Res., 80, 88–98, https://doi.org/10.1016/j.yqres.2013.02.002, 2013.

Liakka, J., Löfverström, M., and Colleoni, F.: The impact of the North American glacial topography on the evolution of the Eurasian ice sheet over the last glacial cycle, Clim. Past, 12, 1225–1241, https://doi.org/10.5194/cp-12-1225-2016, 2016.

Löfverström, M., Caballero, R., Nilsson, J., and Messori, G.: Stationary Wave Reflection as a Mechanism for Zonalizing the Atlantic Winter Jet at the LGM, J. Atmos. Sci., 73, 3329–3342, https://doi.org/10.1175/JAS-D-15-0295.1, 2016.

Löfverström, M., Thompson, D. M., Otto-Bliesner, B. L., and Brady, E. C.: The importance of Canadian Arctic Archipelago gateways for glacial expansion in Scandinavia, Nat. Geosci, 15, 482-488, https://doi.org/10.1038/s41561-022-00956-9, 2022.

Martin, M. A., Winkelmann, R., Haseloff, M., Albrecht, T., Bueler, E., Khroulev, C., and Levermann, A.: The Potsdam Parallel Ice Sheet Model (PISM-PIK) – Part 2: Dynamic equilibrium simulation of the Antarctic ice sheet, The Cryosphere, 5, 727–740, https://doi.org/10.5194/tc-5-727-2011, 2011.

Menviel, L. (2019). The southern amplifier. Science, 363, 1040–1041. https://doi.org/10.1126/science.aaw7196

Milankovitch, M.: Kanon der Erdbestrahlung und Seine Andwendung auf das Eiszeitenproblem, Royal Serbian Academy Special Publication, 132, Belgrade, Serbia, 1941.

Niu, L., Lohmann, G., Hinck, S., Gowan, E. J., and Krebs-Kanzow, U.: The sensitivity of Northern Hemisphere ice sheets to atmospheric forcing during the last glacial cycle using PMIP3 models, J. Glaciol., 65, 645–661, https://doi.org/10.1017/jog.2019.42, 2019.

Obase, T., Abe-Ouchi, A. & Saito, F. Abrupt climate changes in the last two deglaciations simulated with different Northern ice sheet discharge and insolation. Sci Rep 11, 22359, https://doi.org/10.1038/s41598-021-01651-2, 2021

Ohmura, A., Calanca, P., Wild, M. and Anklin M.: Precipitation, accumulation and mass balance of the Greenland Ice sheet, Z. Gletscherkd. Glazialgeol., 35(1), 1–20, 1999.

Otto-Bliesner, B. L. and Brady, E. C.: The sensitivity of the climate response to the magnitude and location of freshwater forcing: last glacial maximum experiments, Quaternary Sci. Rev., 29, 56–73, https://doi.org/10.1016/j.quascirev.2009.07.004, 2010.

PAGES Past Interglacials Working Group, o. p.: Interglacials of the last 800,000 years, Rev. Geophys., 54, 162–219, https://doi.org/10.1002/2015RG000482, 2016.

Parrenin, F. and Paillard, D.: Amplitude and phase of glacial cycles from a conceptual model, Earth Planet. Sc. Lett., 214, 243–250, 2003.

Patton, H., Hubbard, A., Andreassen, K., Auriac, A., Whitehouse, P. L., Stroeven, A. P., Shackleton, C., Winsborrow, M., Heyman, J., and Hall, A. M.: Deglaciation of the Eurasian ice sheet complex, Quaternary Sci. Rev., 169, 148–172, https://doi.org/10.1016/j.quascirev.2017.05.019, 2017.

Pattyn, F., Schoof, C., Perichon, L., Hindmarsh, R. C. A., Bueler, E., de Fleurian, B., Durand, G., Gagliardini, O., Gladstone, R., Goldberg, D., Gudmundsson, G. H., Huybrechts, P., Lee, V., Nick, F. M., Payne, A. J., Pollard, D., Rybak, O., Saito, F., and Vieli, A.: Results of the Marine Ice Sheet Model Intercomparison Project, MISMIP, The Cryosphere, 6, 573–588, https://doi.org/10.5194/tc-6-573-2012, 2012.

Pattyn, F., Perichon, L., Durand, G., Favier, L., Gagliardini, O., Hindmarsh, R. C. A., Zwinger, T., Albrecht, T., Cornford, S., Docquier, D., Fürst, J. J., Goldberg, D., Gudmundsson, G. H., Humbert, A., Hütten, M., Huybrechts, P., Jouvet, G., Kleiner, T., Larour, E., Martin, D., Morlighem, M., Payne, A. J., Pollard, D., Rückamp, M., Rybak, O., Seroussi, H., Thoma, M., and Wilkens, N.: Grounding-line migration in plan-view marine ice-sheet models: results of the ice2sea MISMIP3d intercomparison, J. Glaciol., 59, 410–422, https://doi.org/10.3189/2013JoG12J129, 2013.

Pattyn, F.: The paradigm shift in Antarctic ice sheet modelling, Nat. Commun., 9, 2728, https://doi.org/10.1038/s41467-018-05003-z, 2018.

Pausata, F. S. R., Li, C., Wettstein, J. J., Kageyama, M., and Nisancioglu, K. H.: The key role of topography in altering North Atlantic atmospheric circulation during the last glacial period, Clim. Past, 7, 1089–1101, https://doi.org/10.5194/cp-7-1089-2011, 2011.

Peltier, W. R.: The impulse response of a Maxwell Earth, Rev. Geophys., 12, 649–669, https://doi.org/10.1029/RG012i004p00649, 1974.

Peltier, W.: Mantle viscosity and ice-age ice sheet tomography, Science, 273, 1359–1364, https://doi.org/10.1126/science.273.5280.1359, 1996

Pollard, D.: A retrospective look at coupled ice sheet–climate modeling, Climatic Change, 100, 173–194, https://doi.org/10.1007/s10584-010-9830-9, 2010.

Pritchard, H. D., Ligtenberg, S. R. M., Fricker, H. A., Vaughan, D. G., Van Den Broeke, M. R., and Padman, L.: Antarctic ice-sheet loss driven by basal melting of ice shelves, Nature, 484, 502–505, https://doi.org/10.1038/nature10968, 2012.

Quiquet, A., Dumas, C., Paillard, D., Ramstein, G., Ritz, C., and Roche, D. M.: Deglacial Ice Sheet Instabilities Induced by Proglacial Lakes, Geophys. Res. Lett., 48, e2020GL092141, https://doi.org/10.1029/2020GL092141, 2021.

Raymo, M. E. and Mitrovica, J. X.: Collapse of polar ice sheets during the stage 11 interglacial, Nature, 483, 453–456, https://doi.org/10.1038/nature10891, 2012.

Rignot, E. and Jacobs, S.: Rapid Bottom Melting Widespread near Antarctic Ice Sheet Grounding Lines, Science, 296, 2020–2023, https://doi.org/10.1126/science.1070942, 2002.

Roe, G. H. and Lindzen, R. S.: The Mutual Interaction between Continental-Scale Ice Sheets and Atmospheric Stationary Waves., J. Climate, 14, 1450–1465, 2001.

Scherrenberg, M. D. W., Berends, C. J., Stap, L. B., and van de Wal, R. S. W.: Modelling feedbacks between the Northern Hemisphere ice sheets and climate during the last glacial cycle, Clim. Past, 19, 399–418, https://doi.org/10.5194/cp-19-399-2023, 2023.

Schoof, C.: Ice sheet grounding line dynamics: Steady states, stability, and hysteresis, J. Geophys. Res., 112, F03S28, https://doi.org/10.1029/2006JF000664, 2007.

Schoof, C.: Marine ice sheet stability, J. Fluid Mech., 698, 62–72, https://doi.org/10.1017/jfm.2012.43, 2012.

https://doi.org/10.5194/cp-2023-42
Preprint. Discussion started: 3 July 2023

Sigman, D., Fripiat, F., Studer, A. S., Kemeny, P. C., Martínez-García, A., Hain, M. P., Ai, X., Wang, X., Ren, H., and Haug, G. H.: The Southern Ocean during the ice ages: A review of the Antarctic surface isolation hypothesis, with comparison to the North Pacific, Quaternary Sci. Rev., 254, 106732, https://doi.org/10.1016/j.quascirev.2020.106732, 2021.

Simms, A. R., Lisiecki, L., Gebbie, G., Whitehouse, P. L., and Clark, J. F.: Balancing the last glacial maximum (LGM) sea level budget, Quatern. Sci. Rev., 205, 143–153, https://doi.org/10.1016/j.quascirev.2018.12.018, 2019.

Simon, K. M. and Riva, R. E.: Uncertainty Estimation in Regional Models of Long-Term GIA Uplift and Sea Level Change: An Overview, J. Geophys. Res.-Solid Earth, 125, e2019JB018983, https://doi.org/10.1029/2019JB018983, 2020.

Spratt, R. M. and Lisiecki, L. E.: A Late Pleistocene sea level stack, Clim. Past, 12, 1079–1092, https://doi.org/10.5194/cp-12-1079-2016, 2016.

Sueyoshi, T., Ohgaito, R., Yamamoto, A., Chikamoto, M. O., Hajima, T., Okajima, H., Yoshimori, M., Abe, M., O'ishi, R., Saito, F., Watanabe, S., Kawamiya, M., and Abe-Ouchi, A.: Set-up of the PMIP3 paleoclimate experiments conducted using an Earth system model, MIROC-ESM, Geosci. Model Dev., 6, 819–836, https://doi.org/10.5194/gmd-6-819-2013, 2013.

Sun, S., Pattyn, F., Simon, E. G., Albrecht, T., Cornford, S., Calov, R., Dumas, C., Gillet-Chaulet, F., Goelzer, H., Golledge, N. R., Greve, R., Hoffman, M. J., Humbert, A., Kazmierczak, E., Kleiner, T., Leguy, G. R., Lipscomb, W. H., Martin, D., Morlighem, M., Nowicki, S., Pollard, D., Price, S., Quiquet, A., Seroussi, H., Schlemm, T., Sutter, J., van de Wal, R. S. W., Winkelmann, R., and Zhang, T.: Antarctic ice sheet response to sudden and sustained ice-shelf collapse (ABUMIP), J. Glaciol., 66, 891–904, https://doi.org/10.1017/jog.2020.67, 2020.

Shepherd, A., Ivins, E., Rignot, E., Smith, B., Van Den Broeke, M., Velicogna, I., Whitehouse, P., Briggs, K., Joughin, I., Krinner, G., Nowicki, S., Payne, T., Scambos, T., Schlegel, N., Geruo, A., Agosta, C., Ahlstrøm, A., Babonis, G., Barletta, V., Blazquez, A., Bonin, J., Csatho, B., Cullather, R., Felikson, D., Fettweis, X., Forsberg, R., Gallee, H., Gardner, A., Gilbert, L., Groh, A., Gunter, B., Hanna, E., Harig, C., Helm, V., Horvath, A., Horwath, M., Khan, S., Kjeldsen, K. K., Konrad, H., Langen, P., Lecavalier, B., Loomis, B., Luthcke, S., McMillan, M., Melini, D., Mernild, S., Mohajerani, Y., Moore, P., Mouginot, J., Moyano, G., Muir, A., Nagler, T., Nield, G., Nilsson, J., Noel, B., Otosaka, I., Pattle, M. E., Peltier, W. R., Pie, N., Rietbroek, R., Rott, H., Sandberg-Sørensen, L., Sasgen, I., Save, H., Scheuchl, B., Schrama, E., Schröder, L., Seo, K. W., Simonsen, S., Slater, T., Spada, G., Sutterley, T., Talpe, M., Tarasov, L., Van De Berg, W. J., Van Der Wal, W., Van Wessem, M., Vishwakarma, B. D., Wiese, D., and Wouters, B.: Mass balance of the Antarctic Ice Sheet from 1992 to 2017, Nature, 558, 219–222, https://doi.org/10.1038/s41586-018-0179-y, 2018.

Ullman, D. J., LeGrande, A. N., Carlson, A. E., Anslow, F. S., and Licciardi, J. M.: Assessing the impact of Laurentide Ice Sheet topography on glacial climate, Clim. Past, 10, 487–507, https://doi.org/10.5194/cp-10-487-2014, 2014.

Upham, W.: The geology of central and western Minnesota. A preliminary report. By Warren Upham, assistant on the Geological and Natural History Survey of the state, under the direction of Prof. N. H. Winchell. [From the General Report of Progress for the Year 1879], St. Paul, The Pioneer Press Co., 1880

Uppala, S. M., Kållberg, P. W., Simmons, A. J., Andrae, U., da Costa Bechtold, V., Fiorino, M., Gibson, J. K., Haseler, J., Hernandez, A., Kelly, G. A., Li, X., Onogi, K., Saarinen, S., Sokka, N., Allan, R. P., Andersson, E., Arpe, K., Balmaseda,

https://doi.org/10.5194/cp-2023-42
Preprint. Discussion started: 3 July 2023

M. A., Beljaars, A. C. M., van de Berg, L., Bidlot, J., Bormann, N., Caires, S., Chevallier, F., Dethof, A., Dragosavac, M., Fisher, M., Fuentes, M., Hagemann, S., Hólm, E., Hoskins, B. J., Isaksen, L., Janssen, P. A. E. M., Jenne, R., McNally, A. P., Mahfouf, J.-F., Morcrette, J.-J., Rayner, N. A., Saunders, R. W., Simon, P., Sterl, A., Trenberth, K. E., Untch, A., Vasiljevic, D., Viterbo, P., and Woollen, J.: The ERA-40 re-analysis, Q. J. Roy. Meteor. Soc., 131, 2961–3012, 2005.

Weertman, J.: Stability of the Junction of an Ice Sheet and an Ice Shelf, J. Glaciol., 13, 3–11, https://doi.org/10.3189/S0022143000023327, 1974.

Yamamoto, M., Clemens, S.C., Seki, O. et al. Increased interglacial atmospheric CO2levels followed the mid-Pleistocene Transition. Nat. Geosci. 15, 307–313 (2022). https://doi.org/10.1038/s41561-022-00918-1

https://doi.org/10.5194/cp-2023-42
Preprint. Discussion started: 3 July 2023

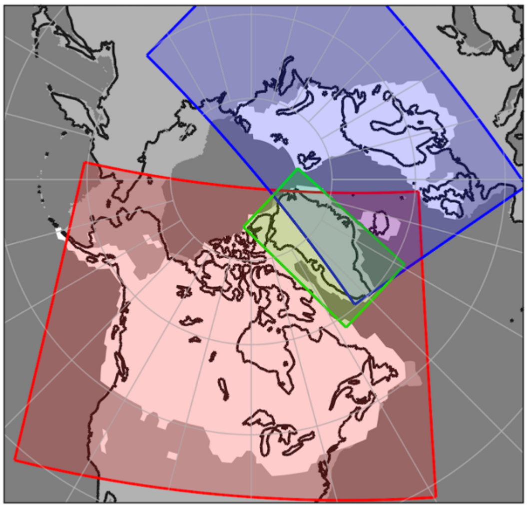

Figure 1. The extent of the North American (red), Greenland (green) and Eurasian (blue) domains. The present-day coastline is shown (black lines), as well as the LGM land and ocean (shown in grey). The extent of the LGM ice sheets in Abe-Ouchi et al. (2015) is shown in white.

https://doi.org/10.5194/cp-2023-42
Preprint. Discussion started: 3 July 2023

Climate of the Past
Discussions
Open Access

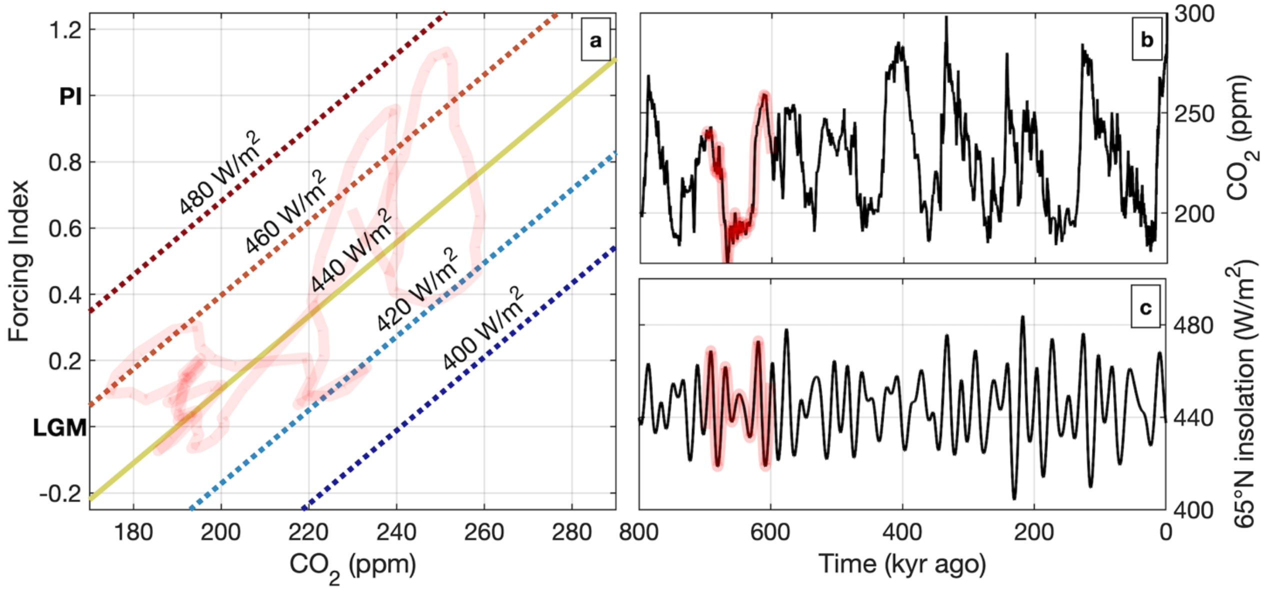

675 **Figure 2.** The forcing index (a), which combined with an albedo feedback, drives temperature changes in the ice-sheet model. The forcing index depends on the prescribed CO_2 (b; Bereiter et al., 2015) and insolation (c; Laskar et al., 2004). The pathway of the forcing-index for a 100-kyr period is shown in red. A forcing index of 0 (1) represents LGM (PI) temperature contribution from external forcing.

https://doi.org/10.5194/cp-2023-42
Preprint. Discussion started: 3 July 2023

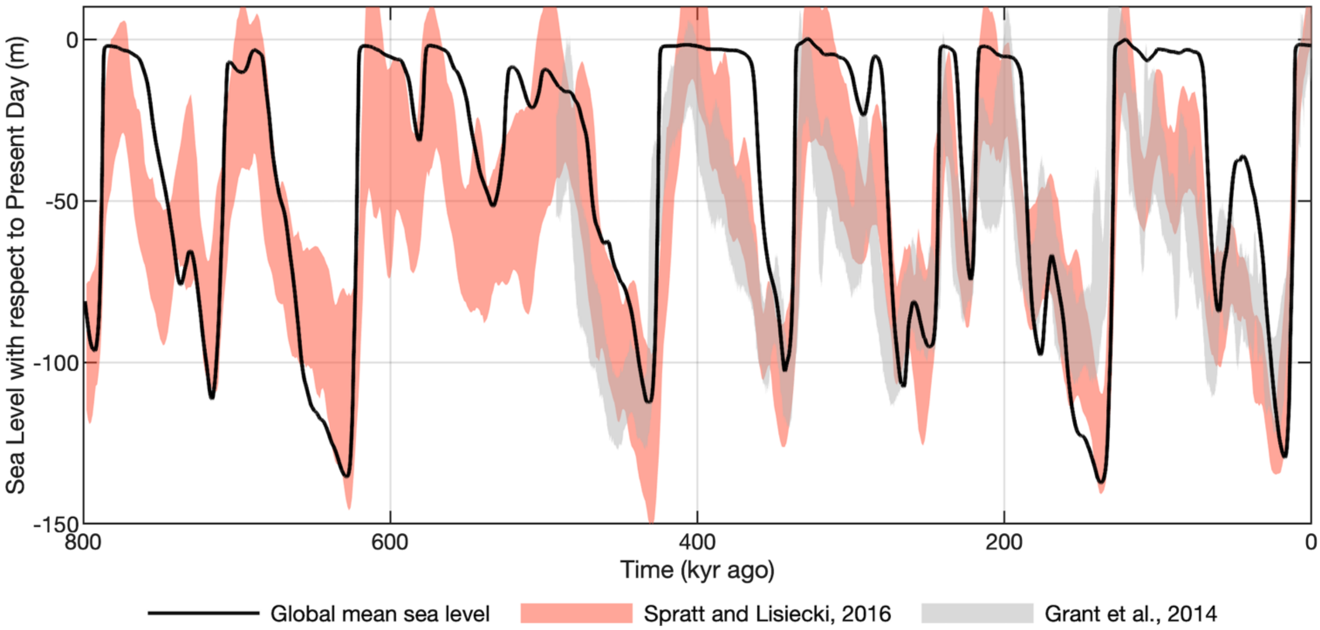

Figure 3. Simulated global mean sea level change compared to Grant et al. (2014) and Spratt and Lisiecki (2016). 30% was added to the Northern Hemisphere ice sheet volume to represent the total sea level change.

https://doi.org/10.5194/cp-2023-42
Preprint. Discussion started: 3 July 2023

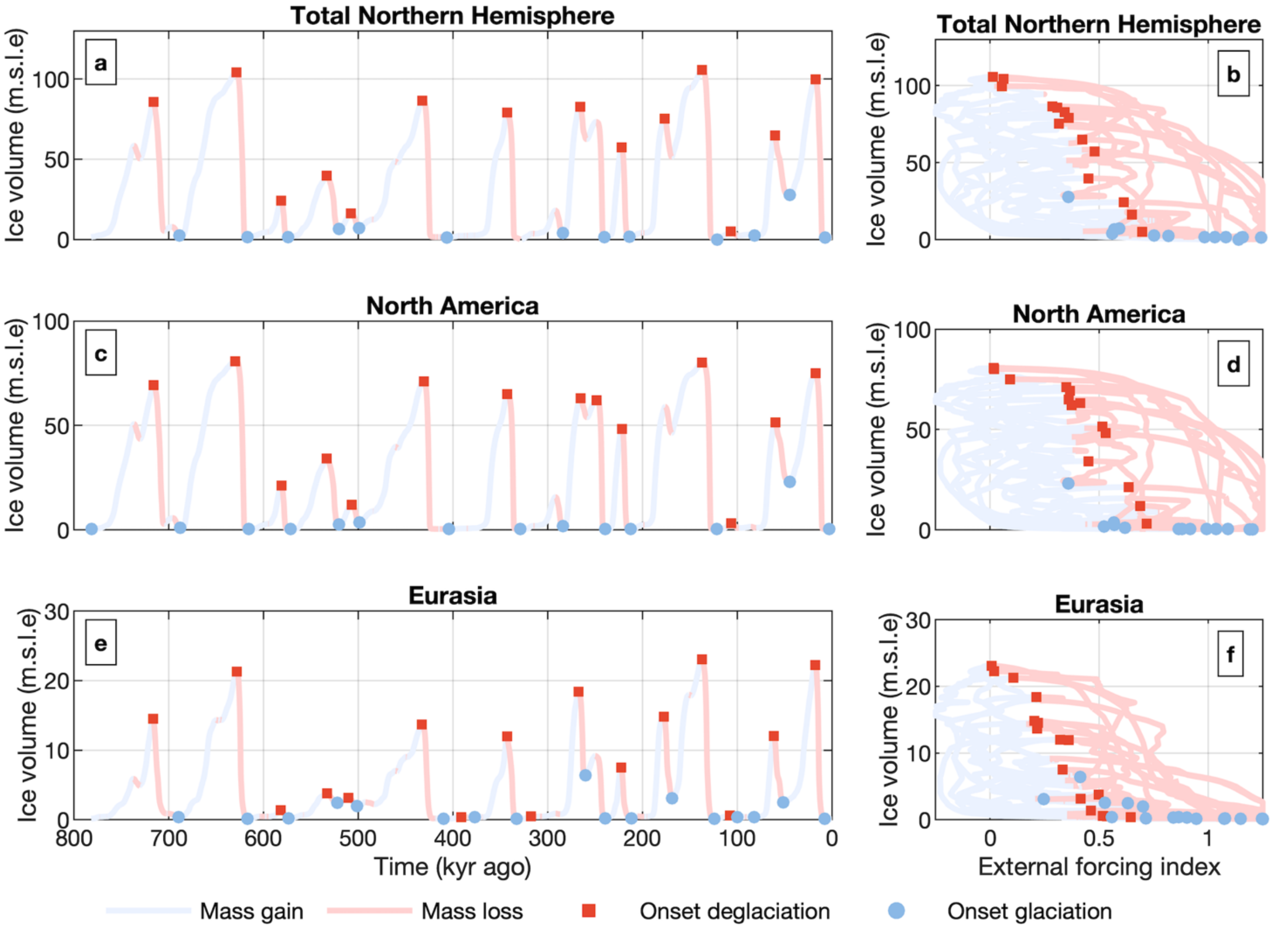

Figure 4. Time series of the simulated ice volume in the Baseline experiment are shown in panels a,c and e. Ice volume is compared to the climate forcing in the panels c,d and f. Panel a,b show the ice volume of Eurasia, Greenland and North America combined, while c, d, e and f only shows one ice sheet per panel. Red colours indicate when an ice sheet is losing mass, while blue shows when an ice sheet gains mass. Blue circles indicate the start of a glaciation, red squares the start of the deglaciation.

https://doi.org/10.5194/cp-2023-42
Preprint. Discussion started: 3 July 2023

Climate of the Past
Discussions

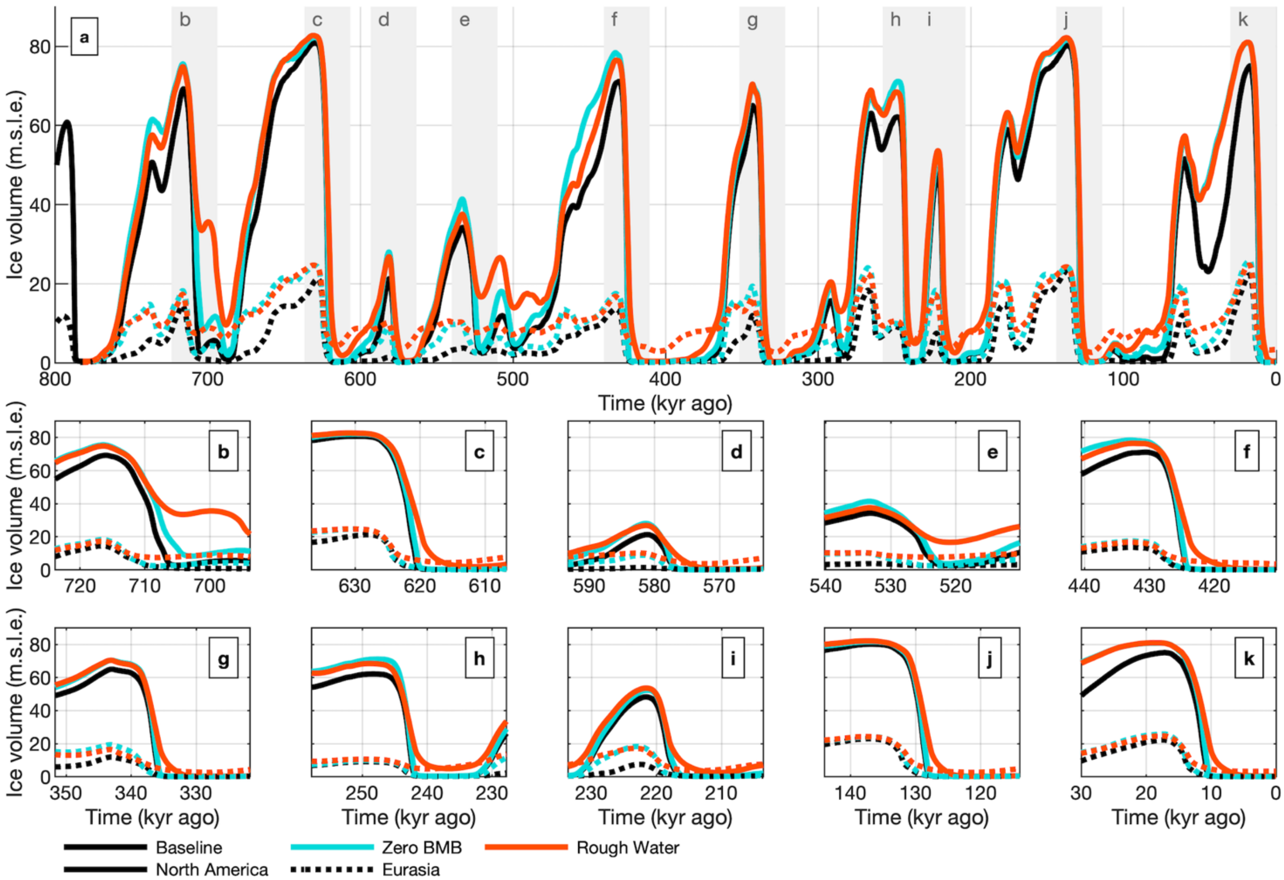

Figure 5. Time-series of the North American and Eurasian ice sheets during various deglacial periods. The full 800 kyr time-series is shown in panel a. The grey patches in panel a correspond to the time-series shown in panels b-k.

https://doi.org/10.5194/cp-2023-42
Preprint. Discussion started: 3 July 2023

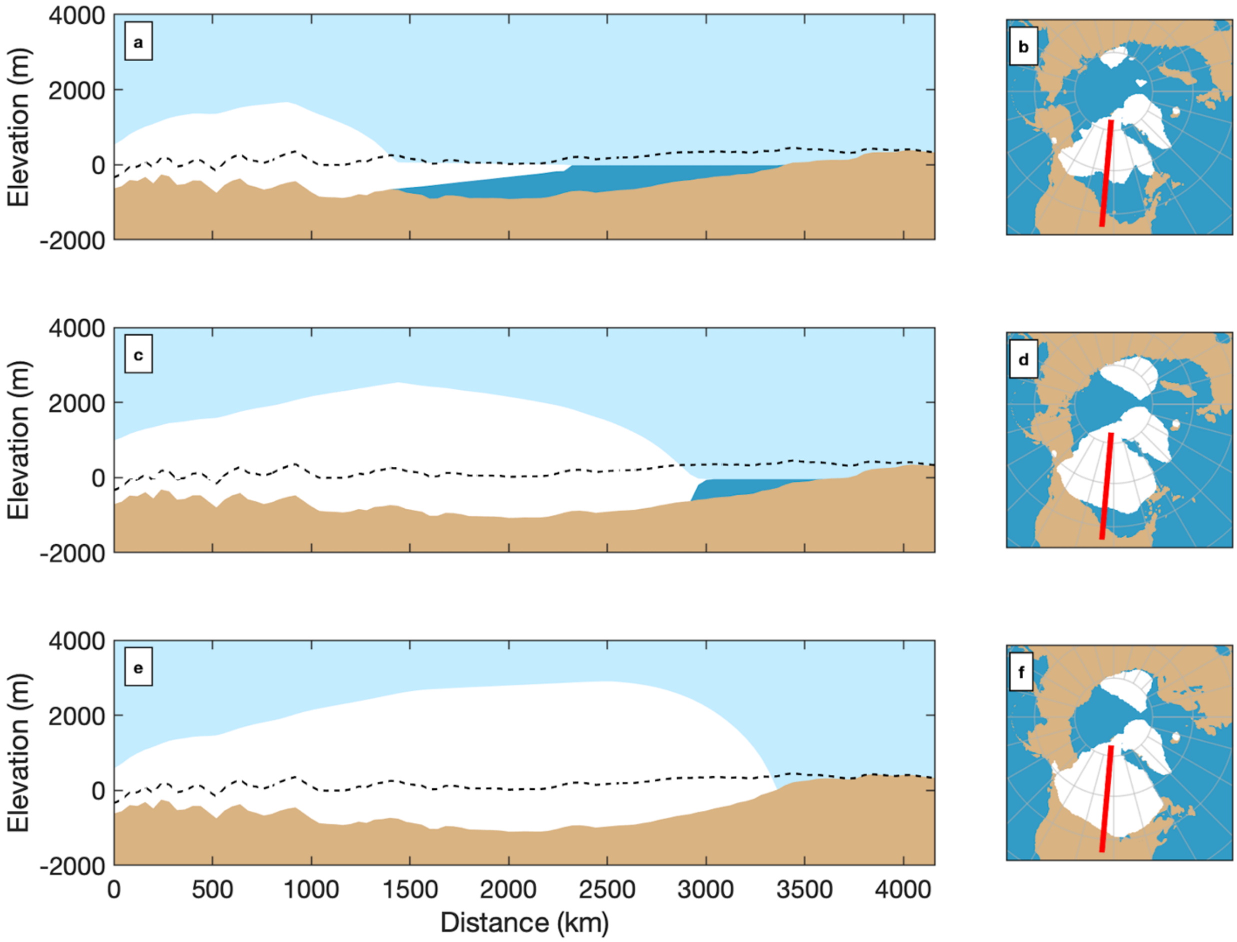

Figure 6. Transects (a,c,e) of the Baseline (a,b) the Rough Water (c,d) and Fast GIA simulations (e,f) at 11 kyr ago. PD bedrock is shown as a dashed line in a,c and e. The 0 km distance represents the Northern-most point of the transect, which is shown in figures b,d and f.

https://doi.org/10.5194/cp-2023-42
Preprint. Discussion started: 3 July 2023

Climate of the Past
Discussions

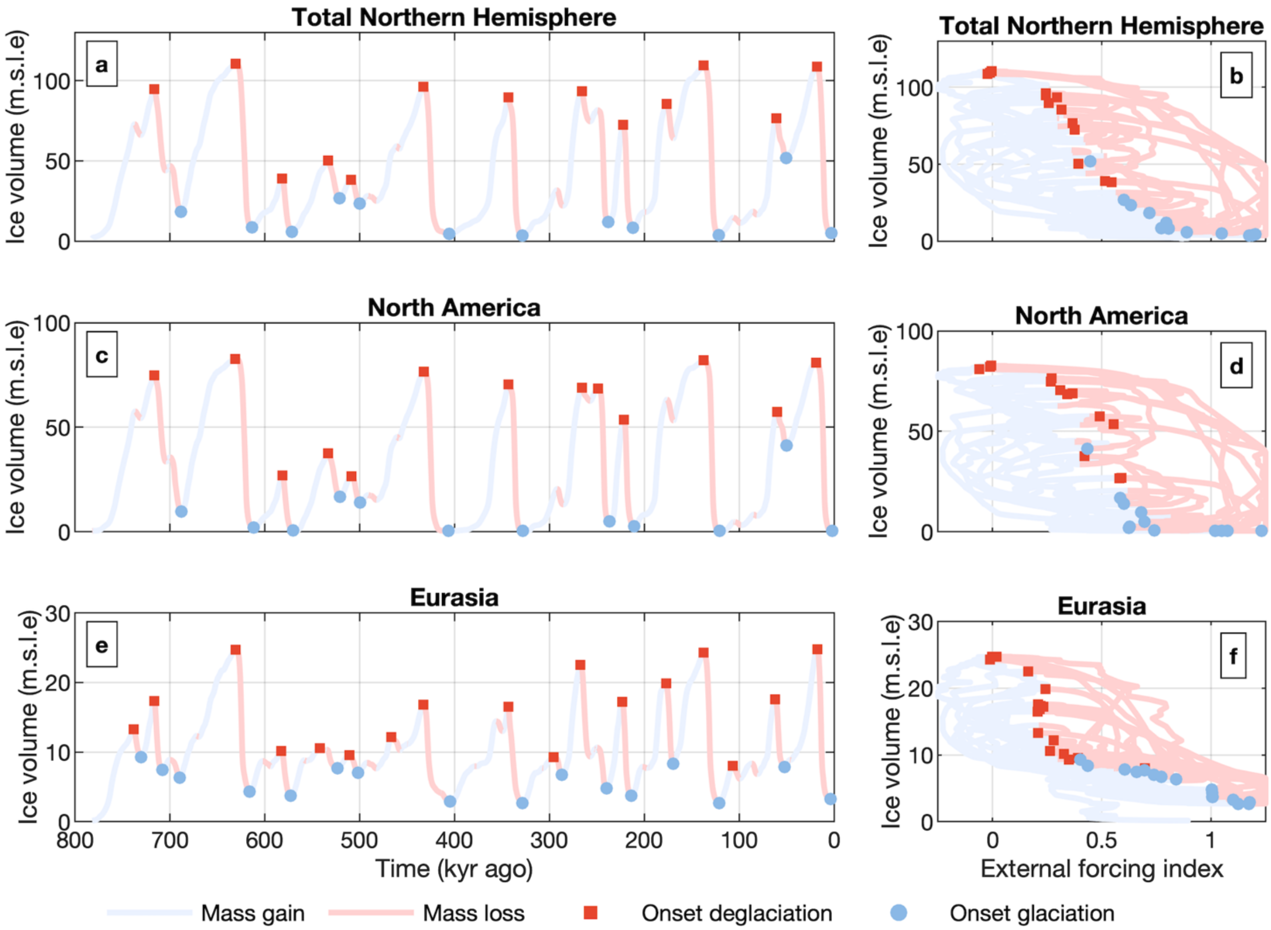

705 **Figure 7.** Time-series of ice volume from the Rough Water simulation are shown in panels a,c and e. Ice volume is compared to the external forcing for the Rough Water simulation in b,d,f. The Eurasian ice sheet does not melt in the Rough Water simulation, with some ice persisting throughout interglacials in the Barents-Kara Sea region. Red indicates mass loss while blue shows mass gain of the ice sheet. Red squares show the onset of a deglaciation event. Blue circles indicate when the ice sheet starts gaining mass.

https://doi.org/10.5194/cp-2023-42
Preprint. Discussion started: 3 July 2023

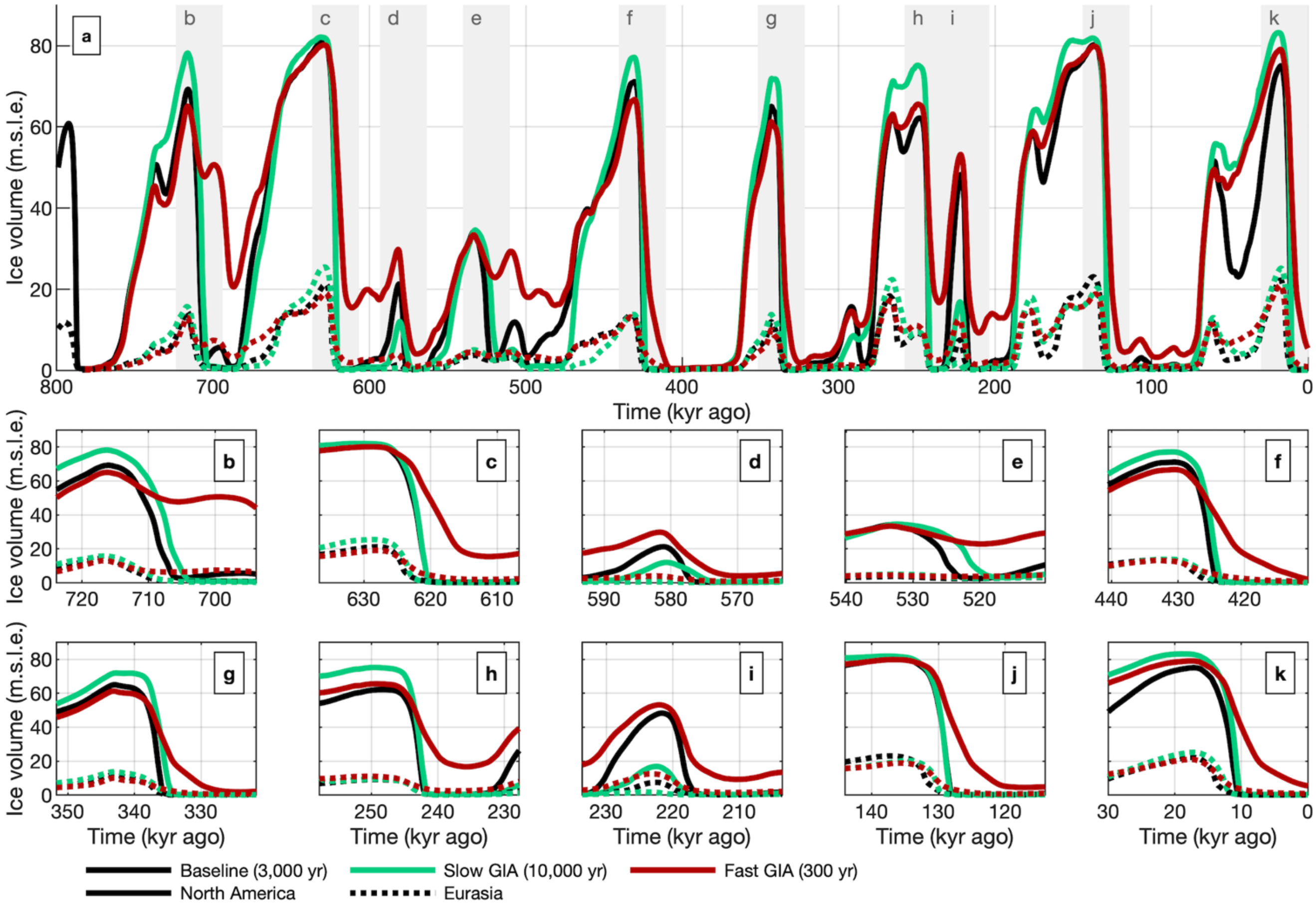

Figure 8. Time-series of ice volume with different GIA relaxation times. The time-series of the past 800 kyr is shown in panel a. Panels b-k show one termination each, which are indicated by the grey patches in panel a.